Anthropogenic Influence on the Rhine water temperatures

Alex Zavarsky[1] and Lars Duester[1]

[1]Federal Institute of Hydrology, Department G4- Radiology and Monitoring, Koblenz Germany

Correspondence: Alex Zavarsky (alexz@mailbox.org)

Abstract. River temperature is an important parameter for water quality and an important variable for physical, chemical and biological processes. River water is also used by production facilities as cooling agent. We introduce a new way of calculating a catchment-wide air temperature and regressing river temperature vs air temperatures. As a result the meteorological influence and the anthropogenic influence can be studied separately. We apply this new method at four monitoring stations (Basel, Worms, Koblenz and Cologne) along the Rhine and show that the long term trend (1979-2018) of river water temperature is, next to the increasing air temperature, mostly influenced by decreasing nuclear power production. Short term changes on time scales < 5 years are due to changes in industrial production. We found significant positive correlations for this relationship.

1 Introduction

River water temperature (T_w) greatly influences the most important physical and chemical processes in rivers and is a key factor for river system health (Delpla et al., 2009). T_w also defines and confines animal habitats (Isaak et al., 2012; Durance and Ormerod, 2009) and the spread of invasive species (Wenger et al., 2011; Hari et al., 2006) and is therefore an important ecological parameter. River water is not solely important from an environmental perspective but is an important means of production. Especially for energy intensive industries such as power plants, oil refineries, paper or steel mills, river water is an important cooling agent. Its availability is a basic requirement for the facilities location (Förster and Lilliestam, 2010). In this context, one has to bear in mind, that given a 32 % energy efficiency, 68 % of the energy used in a facility is discharged through the cooling system into the respective stream (Förster and Lilliestam, 2010). This leads to a significant heat load even on large rivers such as the Rhine (IKSR, 2006; Lange, 2009). As a consequence, anthropogenic heat fluxes (heat discharge) can contribute significantly to the heat budget of a river. The natural influences on T_w are: [1] Meteorology, including sensible heat flux, latent heat flux, radiative heat fluxes; change in riparian vegetation [2] Source temperature, which describes the origin of the water, e.g. snow-fed, glacier-fed, groundwater-fed; [3] Hydrology, which influences the water temperature through the amount of water and the flow velocity; [4] Ground heat flux.

Dependent on data availability, computing power, accuracy and the questions asked, T_w can be modeled in different ways. The common options are statistical models, physical based models and modeling by neural networks. Neural networks use a sample

teaching data set to train artificial neurons the relationship between input (e.g. air temperature) and output (T_w) (Zhu et al., 2018). A physical T_w model (Sinokrot and Stefan, 1993) parameterizes all fluxes mentioned in [1] and [3], adds anthropogenic heat input and collects the hydrological and source boundary conditions [2] and [4]. Each modeled heat flux is then applied to the water mass, initialized with the starting and boundary conditions. However, it is difficult to get a good estimation of these parameters over a larger catchment area. As a consequence, statistical models use air temperature (T_a) as a proxy for sensible, latent and radiative heat fluxes (ground heat flux can be neglected) and establish a $T_a \rightarrow T_w$ relationship through regression. T_a is rather easily available from meteorological networks or reanalysis products. This is a well established method and depending on the complexity, linear or exponential models (Stefan and Preud'homme, 1993; Mohseni et al., 1998; Koch and Grünewald, 2010) are used. Generally the exponential model has advantages due to the better simulation of extremely warm and cold T_w but lacks the clear analytic separation of the influences to T_w. Using linear models, Markovic et al. (2013) show that between 81 % - 90 % of the T_w variability can be described by T_a. 9 % - 19 % can be attributed to hydrological factors (e.g. discharge). The study was done for the Danube and Elbe basin using data from the 1939 to 2008. These two rivers have comparable size and catchment area to the Rhine river. Hybrid models are in between physical based and statistical models. They use physical formulation of fluxes but determine their parameters stochastically (Piccolroaz et al., 2016). Another development are spatial statistical models. They correlate various landscape variables (e.g. elevation, orientation, hill shading, river slope, channel width...) across the catchment area and try to statistically determine their influence on T_w at a certain point. These correlations can be across any distance and do not have to satisfy flow connection or direction in the river system. As a prerequisite, a detailed knowledge about the river system and its characteristics is needed (Jackson et al., 2017a, b). An improvement to spatial statistic models is to recognize rivers as a network of connected segments with a definite flow direction(Hoef et al., 2006; Hoef and Peterson, 2010; Isaak et al., 2010; Peterson and Hoef, 2010; Isaak et al., 2014). Correlation of the variables (e.g. T_a, T_w discharge, ...) which influence other T_w, is weighted on their flow connectivity and euclidean or flow distance. These models can also include time lag considerations using temporal auto correlation (Jackson et al., 2018).

1.1 Rhine

Along the Rhine, up to 12 nuclear power plants (NPP) have caused, for decades, the largest part of anthropogenic heat input (Lange, 2009). The nuclear power production increased in the 1970s and 1980s and reached a peak in the mid 1990s. After the Fukushima disaster in 2011, the German government decided to exit from nuclear power production and the first NPPs were shut down. With this political decision a clear drop on nuclear power production is visible, on top of already decreasing production rates. Currently (July 2019) eight NPPs are operational in the catchment area of the Rhine using (partly) river water as cooling agent. In this publication, we hypothesize that, next to environmental factors, this long term decrease in power production together with short term economic changes have an impact on T_w of the Rhine. This impact might be heterogeonous along the river as the location of industry and NPPs is concentrated at several highly industrialized spots.

To test this hypothesis and assess the varying impact of industry, meteorology and hydrology on the Rhine river temperatures, we want to combine ideas from the spatial correlation models to develop a new method of calculating a representative catchment

air temperature (T_c). T_c and discharge Q is then used in a multiple linear regression $T_c \rightarrow T_w$ (Eq. 1). The model is run on a T_w time series from 1979 to 2018 measured at four Rhine stations (Basel (CH), Worms (DE), Koblenz (DE) and Cologne (DE)). The period from 1979 to 2018 experienced several changes in anthropogenic heat input to the Rhine catchment area, which makes it an interesting scenario to be studied.

$$T_w = a_1 + a_2 \cdot T_c + a_3 \cdot Q \tag{1}$$

a_1, a_2 and a_3 are the resulting regression coefficients which describe the magnitude of the respective fluxes (anthropogenic, meteorological and hydrological). T_c is the newly proposed catchment temperature and Q the discharge at the measurement station. The origin of water, e.g. ground water, snow melt, glacier melt, is included by T_c because data from high elevations (e.g. Alps) is also included. Webb et al. (2003); Markovic et al. (2013) have shown that Q is inversely related to T_w and an important factor in the $T_c \rightarrow T_w$ relationship. Additionally, it functions as measure of how fast a the water mass responds to changes in T_w. Ground heat flux, ground water influx and heat generation due to friction are not included in this model because of the comparable small influence (Sinokrot and Stefan (1993) for Mississippi; Caissie (2006) as review article). Other models such as hybrid models (Toffolon and Piccolroaz, 2015) would create lower RMSE but do not allow for a clear distinction between meteorological, hydrological and anthropogenic input.

Using the multiple regression (Eq. 1), we aim to especially investigate the change of a_1 over time, which we call the Rhine base temperature (RBT). This temperature represents the T_w without the influence of meteorology and discharge. RBT is an indicator for industrial heat input and the use of Rhine water as cooling agent. We hypothesize that its long term change is connected with the electricity production of NPPs and its short term variations is connected with overall industrial production and general economic indicators. Using different time series along the Rhine, we investigate where anthropogenic heat fluxes may influence T_w and may lead to an overall heterogeneous warming rate along the Rhine.

2 Methods

2.1 Water temperature and discharge

We use a data-set of daily averaged T_w and Q from 1979-2018 gathered from different sources (WSA, 2019; BfG, 2019; LfU, 2019; BAFU, 2019). The original data-sets have a 10 min sample frequency. Table (1) lists the respective stations along the Rhine (Col. 1), stream km (Col. 2), data availability (Col. 3), the important tributaries upstream (Col. 4) and the reference (Col. 5). T_w was measured by platinum resistivity sensors (Pt100). The accuracy of theses sensors is commonly ± 0.5 ^{o}C but the precision, which describes the ability to detect temperature changes, is 0.05 ^{o}C. As we focus on the change T_w over time and do not compare the absolute temperature, the accuracy is not essential and the precision is sufficient. Errors inflicted by measuring depth and location in the river are also not influencing the calculation, regarding the aim of this study, as long as the measured T_w is a linearly dependent proxy for the average river temperature. Q is provided as daily averages in m^3s^{-1} by the source in Tab. (1) and usually calculated from river stage).

The original data-sets have already been verified by the respective source but are screened by us for suspicious features. Missing

name	stream km	time period	important tributary upstream	reference
Cologne	KM 690	1.1.1985-31.12.2018	Mosel	WSA (2019)
Koblenz	KM 550	1.1.1978-31.12.2018	Main	BfG (2019)
Worms	KM 443	1.1.1971-31.12.2018	Neckar	LfU (2019)
Basel	KM 170	1.1.1977-31.12.2018	Aare	BAFU (2019)

Table 1. Lists of monitoring stations used in this study. Column two provides the location as Rhine km. Column three provides the data range. The third column names the important upstream tributary and column four names the reference.

data points up to one week are linearly interpolated. Longer data-outages and recurring data-outages are not experienced. The data-set is provided by state and federal operated monitoring stations which usually run backup measurement systems.

2.2 Air temperature

T_a is retrieved from the European Centre for Medium-Range Weatherforcast (ECMWF) Reanalysis Model ERA5. It provides an hourly time resolution of the 2 m T_a on a $\frac{1}{4}^o$ by $\frac{1}{4}^o$ grid. The data-set is available from 1979-2018. We took the hourly T_a output and calculated a daily mean for each grid point between 1979 and 2018 to fit the time resolution of T_w.

2.3 Nuclear Power Plants

The annual electrical power production by NPPs is available from the International Atomic Energy Agency (IAEA) Power Reactor Information System (IAEA, 2019). At most 12 NPPs (1986-1988) were online in the Rhine catchment area. Separate blocks of one NPP are combined. In July 2019 eight were operational. All shutdowns were done in Germany.
From estimates by Lange (2009) and based on personal communication from different sources, the heat input by NPPs to the Rhine is calculated for each monitoring station, Fig. (1). The NPPs in Tab. (2) are included in the heat input calculation through a conversion factor which converts electrical produced power to heat input. NPPs with an exclusive river water cooling system have a conversion factor of three, which is based on the power efficiency of electricity generation. Other factors are estimated depending on the cooling system used and personal communication.

2.3.1 Calculated temperature change

We calculate the expected change in RBT (ΔRBT) based on a change in heat input (ΔHI) by NPPs using the average discharge $\bar{Q}$, the heat capacity of water c_p and the water density ρ, Eq. (2).

$$\Delta RBT = \frac{\Delta HI}{c_p \cdot \bar{Q} \cdot \rho} \tag{2}$$

This approach follows the idea that the heat input of NPPs is essential for the heat budget of the river and significantly alters RBT as other important influences, such as meteorology (a_2) and hydrology (a_3), are excluded by applying the multiple linear regression.

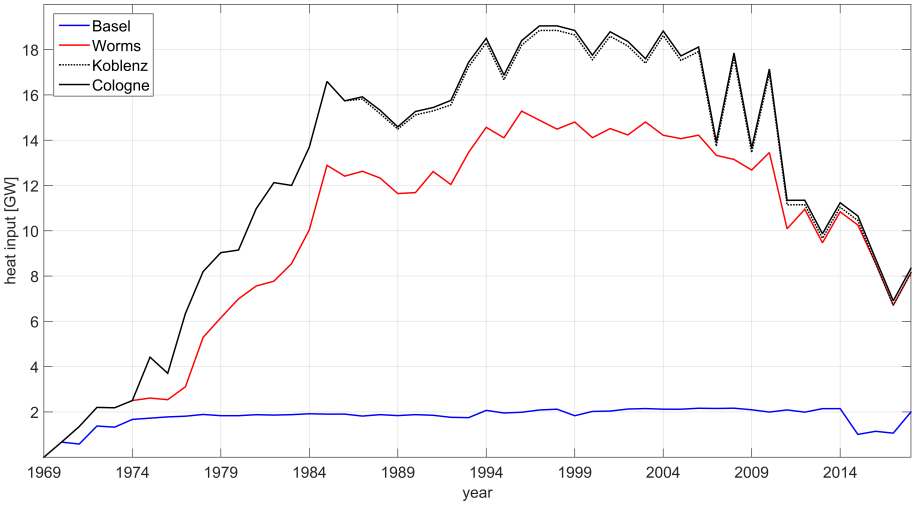

Figure 1. Using the PRIS (IAEA, 2019) database we estimated the heat input by NPPs from 1969 to 2018. This figure shows the total upstream heat input of each monitoring station.

name	country	river	conversion factor	const. heat input
Beznau I+II	CH	Aaare	3	N/A
Biblis I+II	DE	Rhine	2	N/A
Cattenom I-IV	DE	Mosel	N/A	200 MW
Fessenheim I+II	FR	Rhine	3	N/A
Goesgen	CH	Aare	N/A	50 MW
Grafenrheinfeld	DE	Main	N/A	200 MW
Leibstatt	CH	Rhine	N/A	50 MW
Muehleberg	CH	Aare	3	N/A
Neckarwestheim I+II	DE	Neckar	1	N/A
Obrigheim	DE	Neckar	3	N/A
Philippsburg I+II	DE	Rhine	1	N/A

Table 2. NPPs included in this manuscript. The coversion factor describes the conversion from electrical power generation to heat input. If cooling towers are installed a constant heat input is used based on Lange (2009).

2.4 Gross Domestic Product

The gross domestic product (GDP) for the adjacent German federal states is obtained from VGdL (2019a, b). Due to changes in the calculation method of the GDP before and after the German reunification (1991), two separate data-sets are used. For this study only the GDP-change of the secondary sector (construction and production) is used.

The RBT, if compared to the GDP, is filtered using a 10^{th} order butterworth bandpass filter. The sampling rate of the GDP is

$1\ y^{-1}$. We use $1.1\ y^{-1}$ as higher and $0.05\ y^{-1}$ as lower cutoff frequencies for RBT. This means that signals with a periodicity larger than 20 y and lower than 0.9 y are excluded. The reasoning is to make the RBT data comparable to the yearly data of the GDP-change. The low frequency cutoff is canceling long term trends as a GDP-change is only related to the previous year. The high frequency cutoff is used to dampen fast alternating RBT signals in comparison to the slow sampled GDP data.

2.5 Rescaled adjusted partial sums

Rescaled adjusted partial sums (RAPS) is used to visualize trends in time series which may not be clearly visible in the time series itself. Equation (3) shows the calculation of the RAPS index (X) using a time series Y.

$$X_k = \sum_{i=1}^{i=k} \frac{Y_i - \overline{Y}}{\sigma_Y} \tag{3}$$

$\overline{Y}$ is the average over the total time series, σ is the standard deviation of the whole time series, Y_i is the ith data-point in Y. A change in the slope of the RAPS index only indicates a change in the slope of the original time-series. A negative RAPS slope does not indicate a negative slope in the original time series. Garbrecht and Fernandez (1994); Basarin et al. (2016) used this method to investigate trends in hydrological time series.

2.6 Catchment area

The catchment area is calculated using the Hydrosheds database (Lehner et al., 2008). The $\frac{1}{125}{}^{o}$ by $\frac{1}{125}{}^{o}$ gridded data-set provides information, at each grid point, to which cell the water of a grid cell is drained. Selecting a starting location, e.g. Koblenz at 50.350 ^{o}N and 7.602 ^{o}E it is possible to iteratively identify all grid points draining into this location. These grid points represent the catchment area of this location, in this example Koblenz. By counting the iteration steps, the distance a water drop travels to reach the monitoring station Koblenz is determined. This is done for each station. Additionally, the accumulation number ACC is obtained from the data-set. It defines how many cells in total are draining into a particular cell and is a measure for the size of a river. Finally, a grid, which defines the catchment area, the ACC and the hydrological distance is established spanning the whole catchment area. Figure (2) shows the catchment area, the hydrological distance and the calculated flow time to the Koblenz monitoring station.

Accumulation

ACC is an estimate for the river size. Grid points of large rivers which are fed by many grid points have a large ACC. Figure 3 shows the distribution of the ACC. Each grid points is given the the number of grid points discharging into this very grid point. Large rivers, such as the Rhine, Main, Neckar are easily visible.

2.7 Multiple regression

We use a multiple linear regression to separate the anthropogenic (a_1), meteorological (a_2) and hydrological (a_3) contributions to the river water temperature. T_w is regressed with T_c and river discharge Q. Their regression coefficients a_2 (T_c slope) and

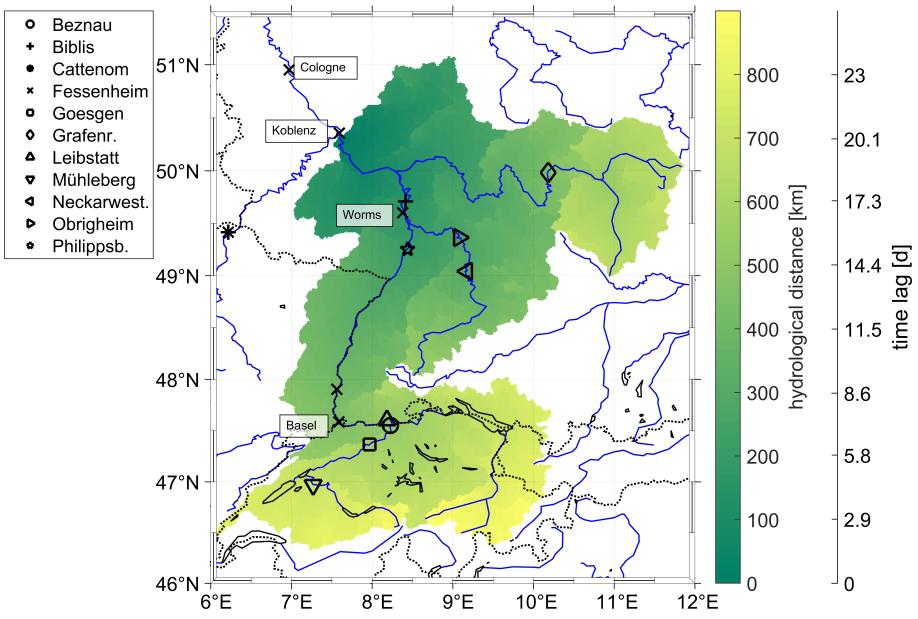

Figure 2. Catchment area of the Koblenz monitoring station. The colors show the hydrological distance between the monitoring station and each grid point of the catchment area. The second y-axis shows the time, in our model, it takes to flow from a grid point to the monitoring station based on the hydrological distance. The flow speed is 0.4 ms^{-1} and in this study constant in space and time. The Xs with the name-tag Basel, Worms, Koblenz and Cologne mark the monitoring stations. The other markers show the location of the NPPs. For names refer to the legend.

a_3 (Q slope) represent the magnitude of the respective influences. The offset a_1 (RBT) combines all other influences, which are controlled by anthropogenic sources.

The linear regression is improved by using a new method for calculating T_c. Instead of taking T_a at the monitoring station, we improve Eq. (1) by a time dependent average of T_a (x,y,t) over the whole, Eq. (4). (x,y) are spatial coordinates in the catchment area and a subscript $_0$ marks the location of the measurement station.

$$T_w(t_0) = a_1 + a_2 \cdot T_c(x, y, t_0 + \Delta t(x, y)) + a_3 \cdot Q(x_0, y_0, t) \tag{4}$$

The new representative catchment temperature is called T_c. The difference between the measurement time t_0 and the reading of T_a is called time lag Δt(x,y) and depends on the hydrological distance between the measurement point and the reading.

Time lag

A change in T_w is slower than a change in T_a. The time lag Δt describes this lagging and is commonly used in water temperature models.

A reason for the occurrence of Δt is that the water mass' mixing capability, heat capacity and surface area cause a strong thermal inertia. Changing T_w through new meteorological conditions and heat fluxes take time. Therefore, linear as well as

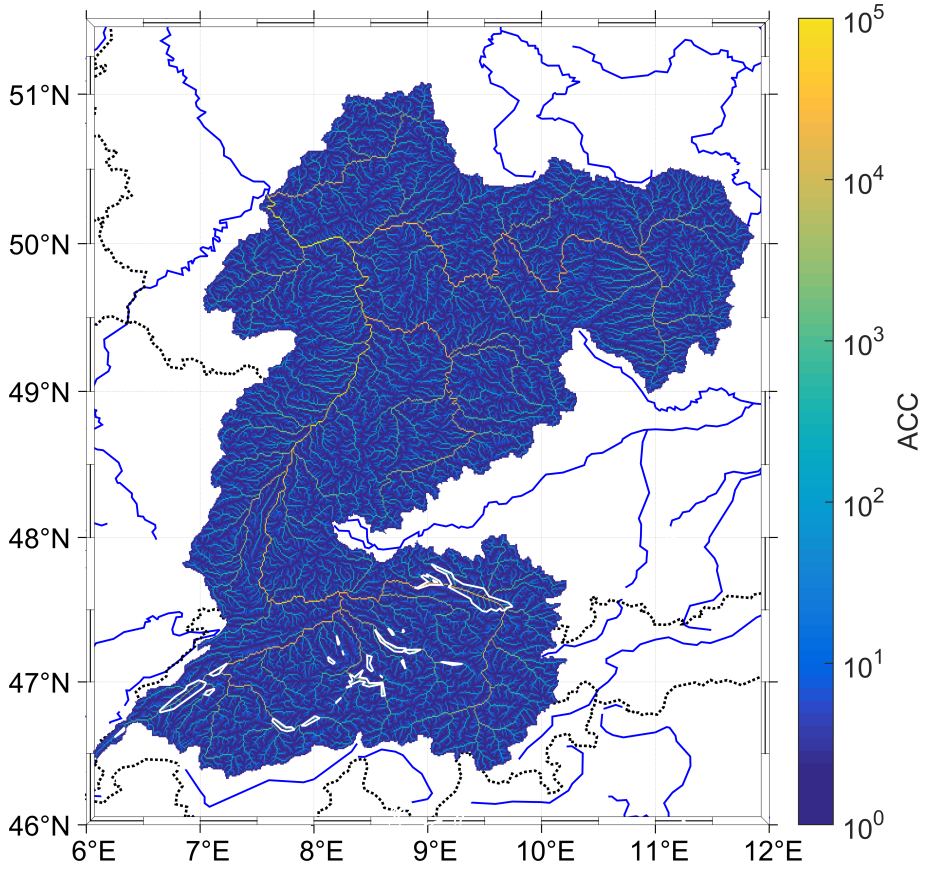

Figure 3. Catchment area of the Koblenz monitoring station. The colors show the number of grid points flowing into the specific gird point

exponential models either use a fixed Δt for T_a (Eq. 5) or an average of T_a including a time span before (Eq. 6) (Stefan and Preud'homme, 1993; Webb and Nobilis, 1995, 1997; Haag and Luce, 2008; Benyaha et al., 2008).

$$T(t_0) = T_a(x_0, y_0, t_0 + \Delta t) \tag{5}$$

$$T(t_0) = \sum_{t=t_o}^{t=\Delta t} T_a(x_0, y_0, t_0) \tag{6}$$

A second reason reason for a mismatch is advection. T_a is measured at the same location and the very same time as T_w. Rivers, in this case the Rhine, exhibit current velocities which enable its water to cover significant distances on time scales larger than days. Therefore it is necessary to take the change of T_a, in space and time, during advection into account. This is especially important for daily averaged T_w (Erickson and Stefan, 2000). Pohle et al. (2019) average eight days of hydroclimatic variables over the whole catchment area, Eq. (7). However, this approach does not include the characteristics of flow path and flow speed.

Δt [d]	weighing factor	distance from measurement point [km]
0	1	0
-1.01	0.96	35.1
-2.00	0.92	69.6
-5.02	0.81	174.6
	...	
-13.01	0.50	452.5
	...	
-26	0	904

Table 3. This table defines the weighing factors for the distance and the resulting Δt for the monitoring station Koblenz. Δt is calculated from distance and flow speed, Eq. (8). The weighing coefficient is linearly correlated to the Δt.

$$T(t_0) = \sum_{x=0,y=0,t=0}^{x=n,y=m,t=8} T_a(x,y,t) \tag{7}$$

We combine and extend both ideas (Eq. 5, 6 and 7) and average T_a over the whole catchment area but each grid point is linked to a specific time lag $\Delta t(x,y)$. $\Delta t(x,y)$ is dependent on a fixed flow speed v and the hydrological distance s(x,y) to the measurement point, Fig. (2). The distance is obtained from the discharge map (Sec. 2.6) and calculated with v as desctribed by Eq. (8).

$$\Delta t(x,y) = -\frac{s(x,y)}{v} \tag{8}$$

Weighing coefficients

Tobler (1970) proposed that close spatial and temporal conditions tend to be higher correlated than those further away. This leads to the introduction of the weighing factor w. We use a linear decreasing weighing factor from 1 to 0 . 1 is given the grid point closest (smallest Δt) to the monitoring station and 0 the point farthest away (largest Δt). As the size of the catchment area is different for the four monitoring station, four weight coefficient tables are calculated. Table (3) shows the weighing coefficient for Koblenz, as an example.

For reasons of simplification, a catchment-wide hydrological flow model is not used estimating the flow speed at every grid point for every hydrological scenario. Therefore, the flow speed of 0.4 ms^{-1} is set constant. This flow speed is determined by calculating RMSE with a step wise reduction of the flow speed from 1.5 ms^{-1} to 0.3 ms^{-1}. The lowest RMSE at Koblenz is obtained at 0.4 ms^{-1}. The weighing coefficient w is combined with ACC. ACC is used as a second coefficient which over-weighs grid points with large accumulation and therefore large water masses. This ensures a balance between the large number of low ACC grid points, which carry less water, with the influence of T_a on large water masses. Figure (4) shows the product

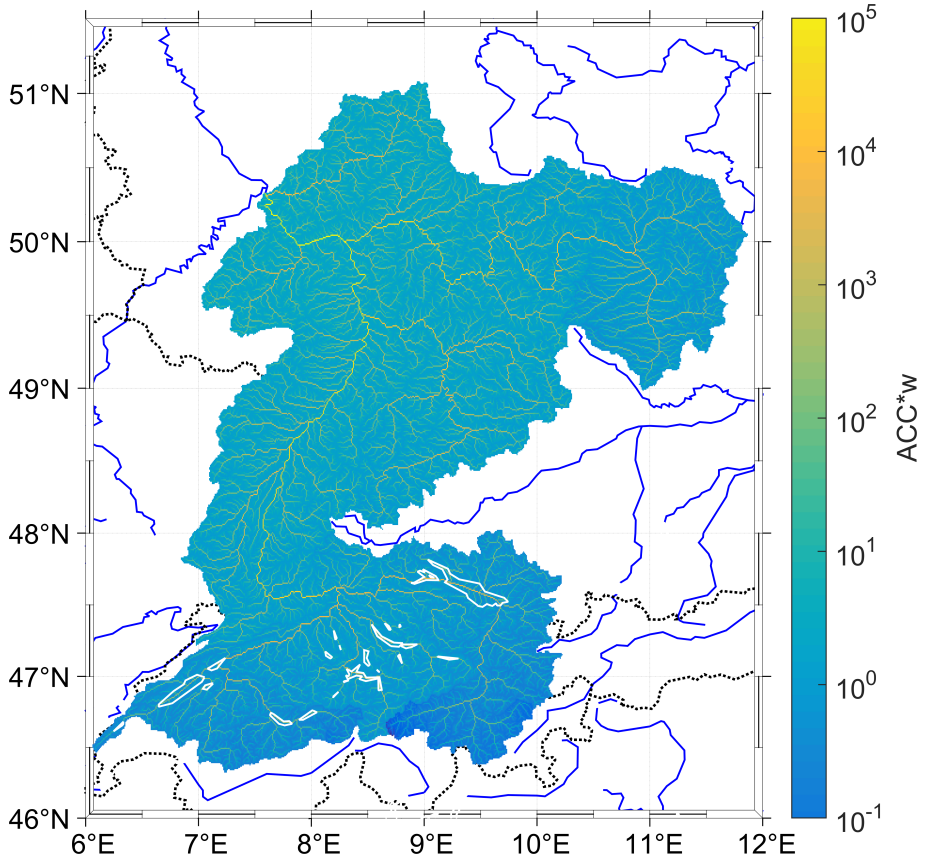

Figure 4. Catchment area of the Koblenz monitoring station. The colors show ACC multiplied with w, which is depending on the distance (Δt).

of ACC and w over the whole catchment area of Koblenz. We also calculate the number of grid points in several ACC bins. The red bars in Fig. (5) show the relative contribution of each ACC group using only their quantity without ACC*w weighing. This shows that the large amount of low ACC (small water mass) grid points would have a large influence over large ACC (e.g. large water masses, rivers, lakes) grid points. The difference is four powers of magnitude. The white bars show the relative contribution using the ACC*w weighing. This distribution gives rather equal importance to all grid points as it puts more weight on grid points covering lakes and rivers. The average difference is about 1 power of magnitude.

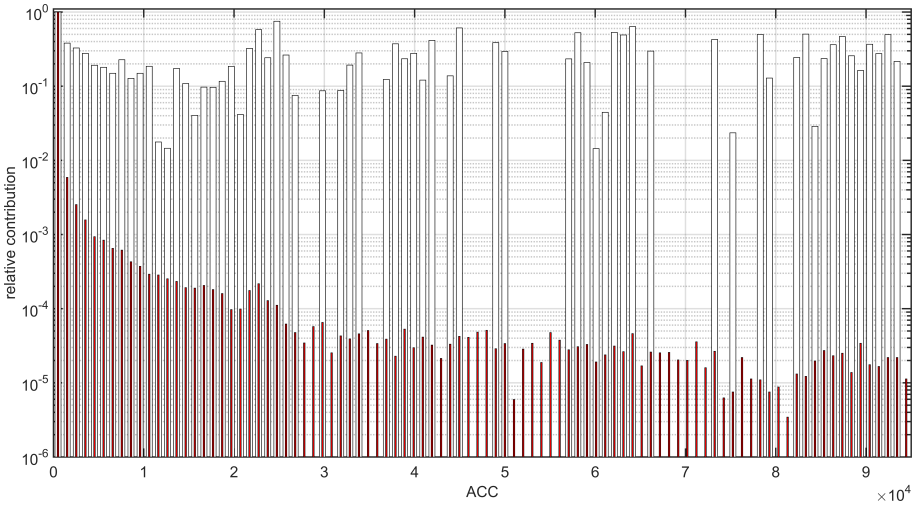

Figure 5. ACC bins (x.axis) vs the relative contribution. The red bars show the relative contribution using by number only. The white bars show the distribution using the weighing ACC*w.

T_c

Combining Δt with ACC*w weighing and the gridded temperature reanalysis data of Sec. (2.2), we propose this new 3D (x, y, t) averaging of T_a shown in, Eq. (9).

$$T_c(t_0) = \frac{1}{\sum w(\Delta t(x,y)) \cdot ACC(x,y)} \sum_{x=1,y=1}^{x=n,y=m} w(\Delta t(x,y)) \cdot ACC(x,y) \cdot T_a(x,y,t_0 + \Delta t(x,y)) \tag{9}$$

$T_c(t)$ is calculated by weighted (ACC*w) averaging $T_a(x,y,t)$ over all grid points of the catchment area (x=1,...n y=1,...m) which reach at the monitoring station at time t_0. The time lag Δt is an estimate for the time it takes for a water droplet from a specific grid point x,y in the catchment area to the measurement location. Based on Eq. (9), we calculated the daily T_c for each monitoring station. This temperature represents the meteorological influence all water droplets have experienced on their way to the monitoring station and is subsequently used in the multiple linear regression.

T_c calculation methods

We additionally use these four calculations methods, [1] w+Δt; [2] avg+Δt; [3] avg; [4] point, to compare their results of the linear regression to the calculation proposed in Eq. (9).

[1] We use only the w weight (Eq. 10) with time lag.

$$T_c(t_0) = \frac{1}{\sum w(\Delta t(x,y))} \sum_{x=1,y=1}^{x=n,y=m} w(\Delta t(x,y)) \cdot T_a(x,y,t_0 + \Delta t(x,y)) \tag{10}$$

[2] No weight, only time lag is used, Eq. (11).

$$T_c(t_0) = \sum_{x=1,y=1}^{x=n,y=m} T_a(x, y, t_0 + \Delta t(x, y)) \tag{11}$$

[3] We calculate a mean $T_a(x, y, t_0)$ over the whole catchment area at the time t_0 of the measurement, Eq. (12). Δt is not used here.

$$w(x, y) = 1 \qquad T_c(t) = \frac{1}{n \cdot m} \sum_{x=1,y=1}^{x=n,y=m} T_a(x, y, t_0) \tag{12}$$

[4] The fourth method uses $T_a(x_0, y_0, t_0)$ at the location x_0, y_0 and time t_0 of the measurement, Eq. (13).

$$T_c(t) = T_a(x_0, y_0, t_0) \tag{13}$$

3 Results

3.1 Water temperature time series

To investigate the long term change over time, we fit a time dependent linear function to the time series of T_w and T_a (catchment average) of all four monitoring stations (Basel, Worms, Koblenz, Cologne). The same is also done, when all four monitoring stations have an overlapping data-set (1985-2018). The left column of Fig. (6) shows the yearly averaged T_w and the linear fits to the two time periods. The average T_a of the catchment area is also shown. The right column of Fig. (6) shows the RAPS index of T_a as well as T_w. The fit coefficients and the rate of warming per year are shown in Tab. (4). We also calculated the T_a increase in the catchment area of all monitoring stations. These slopes are shown in column four and five of Tab. (4).

Figure (6) and Table (4) show that the change of T_w is heterogenous along the Rhine. The slope at Basel is approx. six times higher (0.0350 ^{o}Cy^{-1}) than the one in Cologne (0.0084 ^{o}Cy^{-1}), comparing only the overlapping data-set. However, during the same period T_a shows similar behavior at these two stations, which is an indication of similar meteorological influence. The T_w warming rate from 1985-2018 for Worms and Koblenz are in between those from Cologne and Basel. These two stations show similar T_a warming rates when comparing to Basel and Cologne. Generally, the T_a warming rates are less than 5 % different from each other. The R^2 also shows differences between the measurement stations. Basel exhibits the largest R^2 values and these are consistently high for T_a and T_w. This is in contrast to the station Cologne, where R^2 of T_w is low and insignificant. The slope of T_a at Cologne is lower than at the other stations but still significant. For T_a the RAPS indexes of all monitoring stations shows four concurrent sections (start-1987; 1987-2000; 2000-2014; 2014-end). Their borders are marked by the blue triangles in Fig. (6). The sections represent slope changes of the RAPS index and indicate trend changes in the original time-series. The T_w RAPS index for Basel shows the same pattern of sections as the T_a index. All other stations show a different RAPS T_w to RAPS T_a pattern. This means that the T_a and T_w trends of the original time-series are different at these stations. T_a can not fully describe the trends in T_w.

We hypothesize that different meteorological conditions are not the reason for this difference. Meteorological differences

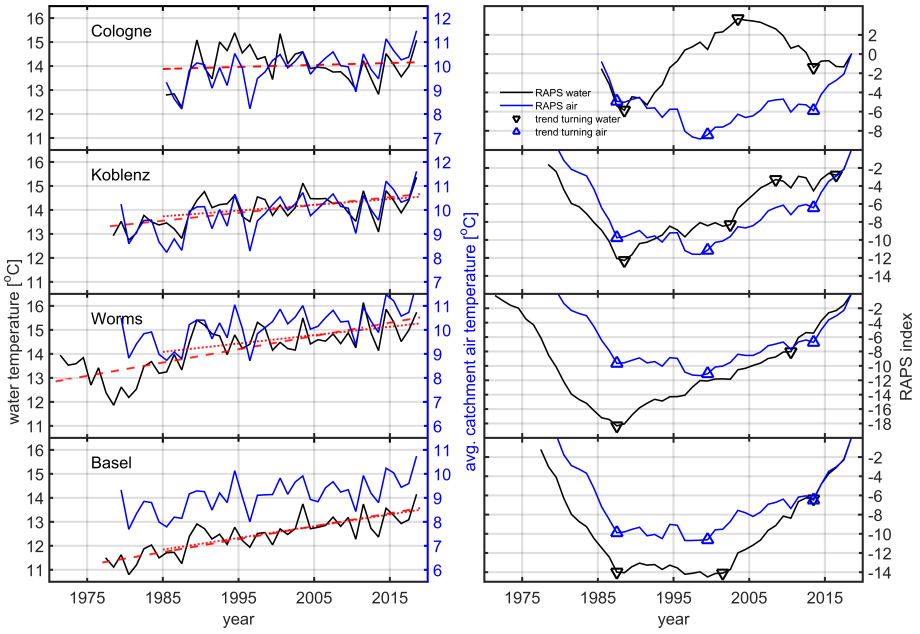

Figure 6. Left column: Yearly averages of water temperatures at four monitoring stations (black line). The red dashed line is a fit to the available data-set. The red dotted line is a fit to the overlapping time period. The blue line is the average air temperature of the catchment area. Right Column: RAPS T_w (black) and T_a (blue) indexes. The triangle markers divide the RAPS index into sections based on a slope change in the RAPS index. Each section also represent a trend change in the original T_a and T_w time-series.

name	slope T_w whole data-set [^{o}Cy^{-1}]	slope T_w 1985-2018 [^{o}Cy^{-1}]	slope T_a whole data-set [^{o}Cy^{-1}]	slope T_a 1985-2018 [^{o}Cy^{-1}]
Basel	$0.054, R^2 = 0.66$	$0.049, R^2 = 0.38$	$0.050, R^2 = 0.48$	$0.050, R^2 = 0.32$
Worms	$0.055, R^2 = 0.52$	$0.035, R^2 = 0.38$	$0.050, R^2 = 0.20$	$0.048, R^2 = 0.36$
Koblenz	$0.033, R^2 = 0.31$	$0.024, R^2 = 0.38$	$0.052, R^2 = 0.11$	$0.048, R^2 = 0.36$
Cologne	$0.008, R^2 = 0.001$	$0.008, R^2 = 0.31$	$0.050, R^2 = 0.001$	$0.050, R^2 = 0.31$

Table 4. Slope of the linear fits to the daily temperature data. The second column is a fit to the available T_w data-set. The third column is a fit to the overlapping T_w data-set from 1985-2018. The fourth column is the rate of T_a increase in the respective catchment area during the whole data-set. The fifth column is the rate of T_a increase in the respective catchment area from 1985-2018. Next to the slope values are the R^2 values, which are statistical significant only if $R^2 > 1.99$

should be visible in the T_a warming rate of the four stations, which is not the case. T_a and T_w RAPS only correspond for the Basel data-set. Therefore, we applied the regression model (Eq. 4) to investigate the patterns of T_w in relation to T_a along the Rhine river.

	RMSE				NSC			
descr.	Basel	Worms	Koblenz	Cologne	Basel	Worms	Koblenz	Cologne
ACC*w+Δt	1.65	**1.24**	**1.02**	**1.41**	**0.93**	**0.96**	**0.97**	**0.95**
(1) w+Δt	**1.56**	1.33	1.43	1.86	0.92	0.95	0.95	0.92
(2) avg+Δt	1.61	1.45	1.70	2.01	**0.93**	0.94	0.93	0.90
(3) avg	2.48	2.43	2.37	2.97	0.82	0.84	0.86	0.79
(4) point	2.73	2.55	2.63	2.85	0.78	0.82	0.82	0.80

Table 5. RSME [^oC] and NSC for all T_c calculation method.The regressions are applied over the total data-set. The first column contains the calculation method number and the method short description. The best results for each monitoring station and each calculation method are bold.

3.2 RBT, long and short term trends

We fit the multiple regression model (Eq. 4), using T_c and Q to T_w of each monitoring station for the available data-set. Afterwards, we recalculate T_w using the regression coefficients a_1, a_2 and a_3. From the comparison between the modeled and measured T_w, we calculate the root mean square error (RMSE) and the Nash-Sutcliffe coefficient (NSC) for each monitoring station, Tab. (5). To support the introduction of weighing coefficients ACC*w and a catchment-wide Δt, we compare five different calculations of T_c from Sec. (2).

Table (5) shows the RMSE and NCS values for all correlations. The lowest (RMSE) and highest (NSC) values are displayed bold in Tab. (5). The lowest RSME is 1.02 ^{o}C for ACC*w+Δt (row one) at the Koblenz station. At this location also the largest NCS of 0.97 appears. We optimized the flow speed for lowest RMSE at the Koblenz station. It is evident that the three methods including a Δt have a lower RMSE (below 2.01 ^{o}C, lowest 1.02 ^{o}C) than the two methods without a Δt (above 2.37 ^{o}C, largest 2.97 ^{o}C). The same trend holds for NCS where the Δt methods are above 0.90 and the other two are below 0.86. We think that the use a catchment-wide Δt improves the quality of the multiple regression analysis and is a significant improvement to $T_a \rightarrow T_w$ based modeling. It is interesting hat combining ACC with the w weighing factor provides the best estimation. Figure (5) could be the reason. Without ACC weighing small water masses (small ACC) are over represented in the contribution to T_c. Large ACC grid points represent large water masses (rivers and lakes) and the influence of T_a on them would be otherwise underestimated.

As the ACC*w+Δt provides the smallest RMSE, this calculation method is used for all further calculations of T_c.

In the supplement we provide a calculation of the regression coefficients for the year 2001 only. These coefficients are used to calculate T_w for each year from 2000 to 2018. The RMSE and NCS data is consistent in magnitude with the long-term regression of this section. The RMSE at Koblenz ranges from 0.75 ^oC to 1.22 ^oC. A lower RMSE is caused by the shorter regression period. This supports the stability and validity of our regression model.

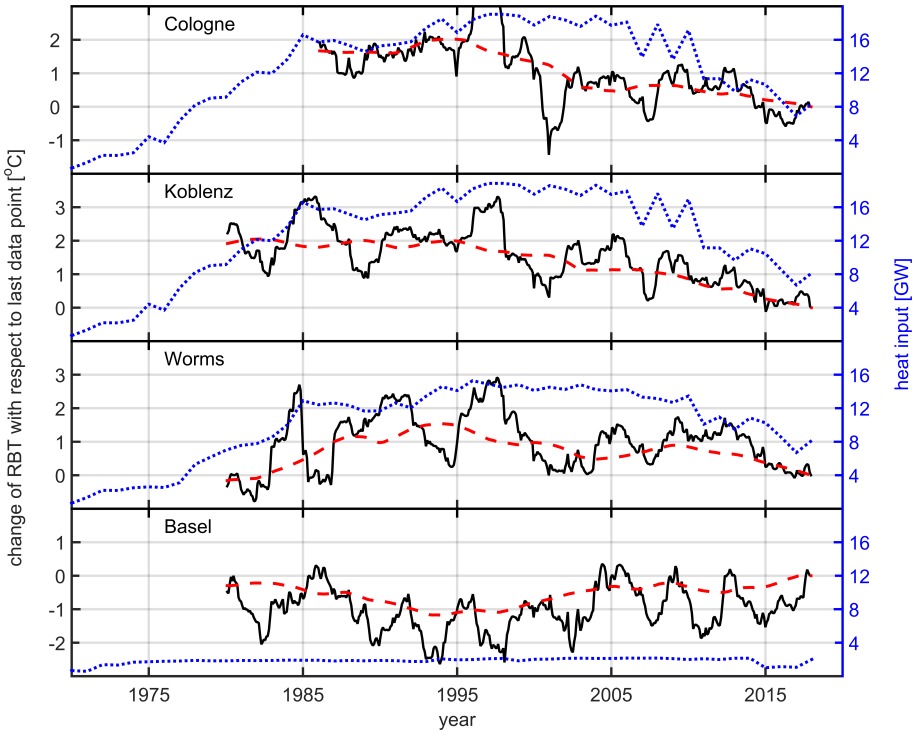

Figure 7. RBT from four monitoring stations (black solid line). The red dashed line is a four year running mean. The blue dotted line is the upstream heat input by NPPs, Sec. (2.3).

3.3 Rhine base temperature

Using the multiple regression in Sec. (3.2), we calculate the coefficients a_1-a_3, Eq. (4). The magnitudes of a_2 and a_3 relate to the influences by meteorology and hydrology (discharge). a_1 is the RBT, which is an indicator for the anthropogenic impact on T_w. We use the RBT to explain differences in the T_w warming rates of Tab. (4).

To point out changes over time, we regress a two year segment of the T_w time series and use a step size of one month to create a RBT time series over the available data-set. As the absolute RBT cannot be meaningfully interpreted, only the changes of RBT over time are shown in Fig. (7). We subtract the last data point of each time series from the rest of the data and show the change of RBT vs time and a four-year running mean. The heat input by NPPs is shown as a dotted blue line with the y-axis on the right hand side.

Long term trend

In this study long term trends occur on time scales of decades. This time scale is on one hand small enough to have significance in this 40 year data-set and on the other hand covers the increase and decrease of nuclear power production.

The heat input by NPPs and the four-year running mean RBT follow a similar trend, Fig. (7). After the maximum of heat

name	period	ΔRBT from data-set	ΔRBT from Eq. (2)	ΔHI [GW]
Basel	2008-2017	-0.26	0.04	0.17
Worms	1996-2017	1.29	1.19	7.14
Koblenz	1999-2017	1.59	1.45	10.5
Cologne	1998-2017	1.21	1.55	10.7

Table 6. Change of RBT (column three) in the period given in column two. The start of the period indicates the maximum heat input of NPPs at the respective measurement station. The calculated temperature change (column four) and the change in HI by nuclear power plants (column five) are also provided. The calculations were done using Eq. (2)

discharge by NPPs between 1996-1998, the heat input as well as the RBT of Worms, Koblenz and Cologne decline. At Basel the RBT as well as the heat input stay comparably constant. To investigate these similar trends we calculate ΔRBT, using Eq. (2), at every station and compare it to the ΔRBT from the measured T_w, Tab. (6). The period for each measurement station starts at the maximum heat input by NPPs for the respective station and ends in the year 2017.

At Basel, both simulated and calculated RBT changes are negligible due to the lack of change in HI. At all other stations, the change in HI is reflected in the change of RBT. The maximum difference between simulation and calculation is 0.34 ^oC.

The change in nuclear power production over a time period of 30 years or more can explain changes and heterogenous warming rates of T_w along the Rhine river. NPPs may also impact T_w at much shorter timer scale but do not seem, to our best knowledge, to change their power output accordingly.

Short term trend

Short term changes (< 5 y) in RBT (Fig. 7) are not influenced by the overall heat in put from NPPs, as they change production at longer time scales, but rather by local industrial conditions, which could also include fossil fuel power plants.

For Basel, we hypothesize that the varying, but without a increasing or decreasing trend over the whole data-set, RBT is influenced by alpine lakes and natural variations. Lakes and reservoirs are to some extend decoupled from the $T_a \rightarrow T_w$ relationship (Erickson and Stefan, 2000). The upper layer (epilimnion) closely follows T_a and the temperature of the larger volume underneath is usually more stable and colder (summer) or warmer (winter). The stratification plays an important role in the outflow temperature of a lake.

For all other stations, we hypothesize that local production facilities and their heat input into the Rhine are responsible for the short term changes. Therefore we compare the RBT time series to economic data. Figure (8) shows the comparison of RBT (black line, one year running mean) vs the changes in the GDP (blue line). A discontinuity in the GDP at 1991 is visible, due to the German reunification, when the calculation method of the GDP changed. Therefore they are plotted as separate lines. For Worms (Fig. 8, bottom panel) we added the change of turnover of the BASF company (red dashed line (AG, 1989)). The BASF is a chemical company. One of its largest production facility, with an estimated heat input of 500 MW to 1 GW, is located 12 km upstream (km 431) from the Worms station. We hypothesize that production and heat input changes of this factory are

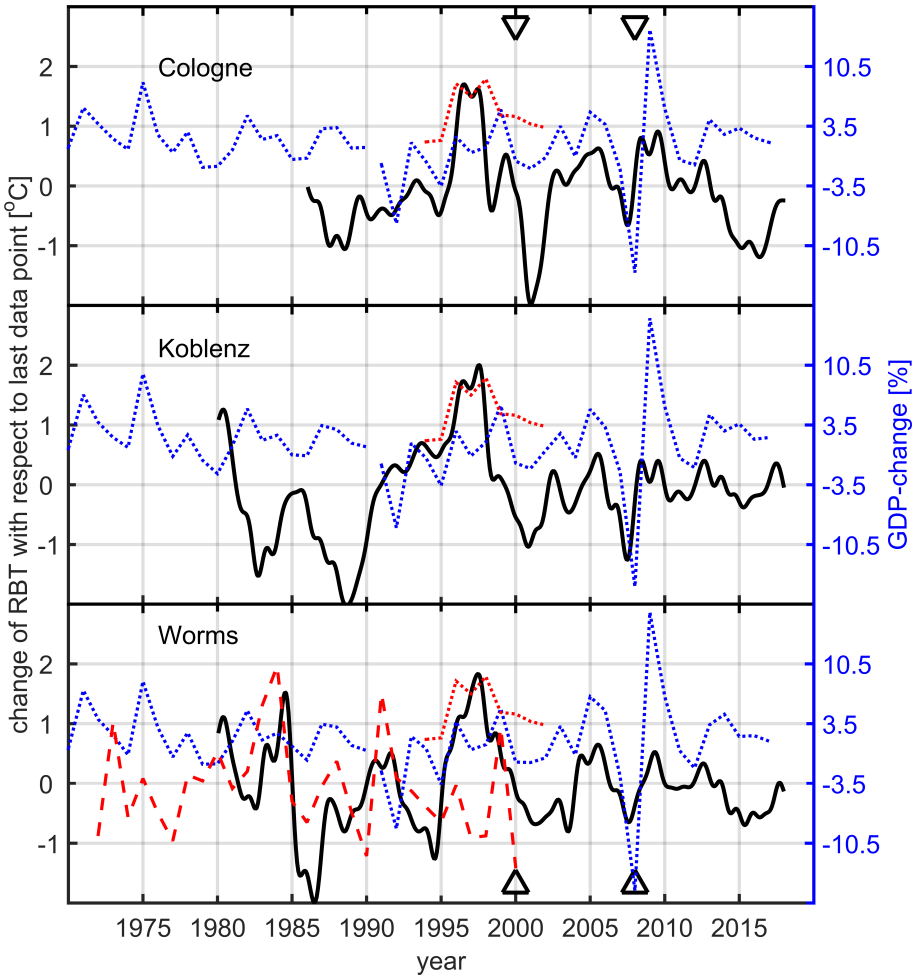

Figure 8. The change of RBT (black solid line) at three monitoring stations (Colgone, Koblenz, Worms). The blue dashed line is the GDP-change of the adjacent federal states. To explain trends during two time periods the red dashed line, which is the turnover of the BASF company, and the red dotted line, production rate of the oil refineries, are added. The triangles mark the years 2000 (burst of the dot-com bubble) and 2008 (mortgage crisis).

also visible. In 1985, although the change in GDP does not indicate a large RBT change, a RBT decrease is visible. This is backed by a turnover decrease in 1985 and 1986. After the German reunification 1991, a negative GDP change (recession) is evident. This is followed by a BASF turnover decline as well as a decrease in RBT. After that, the RBT follows the up and down movements of the GDP, so does the BASF turnover (only shown until 2000). Especially the economic events such as the
305 burst of the dot-com bubble (early 2000s) and the mortgage crisis (2008) are visible in the RBT and the GDP, when a decrease of both parameters followed. The two events are marked with triangles in Fig. (8).

Before 1990, the RBT at Koblenz does not follow the GDP trend and shows a rather anti-cyclic behavior, which can not be

name	ACC*w+Δt	significance
Worms	0.48	p<0.05
Koblenz	0.53	p<0.05
Cologne	0.44	p<0.05

Table 7. Spearman's rank correlations between RBT and GDP-Change for ACC*w+Δt. The last column shows the significance.

explained yet. After 1991, the RBT follows the general trend of the GDP but does not seem to be strongly influenced by the recession after the German reunification. Again, economic events such as the burst of the dot-com bubble (early 2000s) and the mortgage crisis (2008) have influence on the RBT.

The RBT at Cologne does not seem to be strongly influenced by the recession connected to the German reunification, but after 1999 the RBT follows the up and down trends of the GDP.

For all monitoring stations, we added a red dashed line between 1995 and 1999. This dashed line indicates the production rate of German oil refineries (MWV, 2003). From 1995 to 1999 German refineries ran at full capacity level (100%). Usually the capacity levels do not exceed 90%. The increase in production is clearly visible in the RBT of Cologne, where a large oil refinery is located 19 km upstream at km 671 (Rheinland refinery). RBT at Worms and Koblenz could be influenced by the output of a refinery next to Karlsruhe at km 367 (Mineraloelraffinerie Oberrhein).

Correlation

We correlate the GDP-change to the filtered RBT signal. It is noticeable that we must shift the GDP-change 480 days to the past to get matching trends. This means that a change in RBT or anthropogenic heat input appears 480 days earlier than in the GDP calculation. The shift could be caused by two reasons: [1] We are using the GDP difference of two consecutive years, which has a significance at a point of time within these two years. [2] The GDP could be lagging behind the real economic situation, in this case the industrial production. Yamarone (2012) claims that GDP is a coincident economic indicator similar to industrial production. However, he uses quarterly GDP calculations vs our annual data. The quaterly data-set could be reacting faster to changes. A second thought is that he compares industrial production calculations, which is an economic index, to GDP (another economic index). We have basically real time data from the industrial heat input into the river. This shift is not done in Fig. (7) because a shift of 1.5 y on a 40-year time scale is negligible.

Table (7) shows the Spearman's rank correlation coefficients of Worms, Koblenz and Cologne fo rACC*w+Δt calculation method, which produces the lowest RMSE in Koblenz. All correlations are positive and significant (p<0.05). The correlation in Koblenz is the highest. Fig. 9 shows the filtered RBT signal vs the GDP-change at the three monitoring stations. The RBT time-series is detrended and filtered. This graph depicts in detail the correlation of GDP-change and RBT. Most of the time the change in filtered and shifted RBT is coincident, after shifting) with the GDP-change. The RBT peak from 1995-1998 is not very well represented by the GDP-change, which has already been discussed in context of Fig. 8.

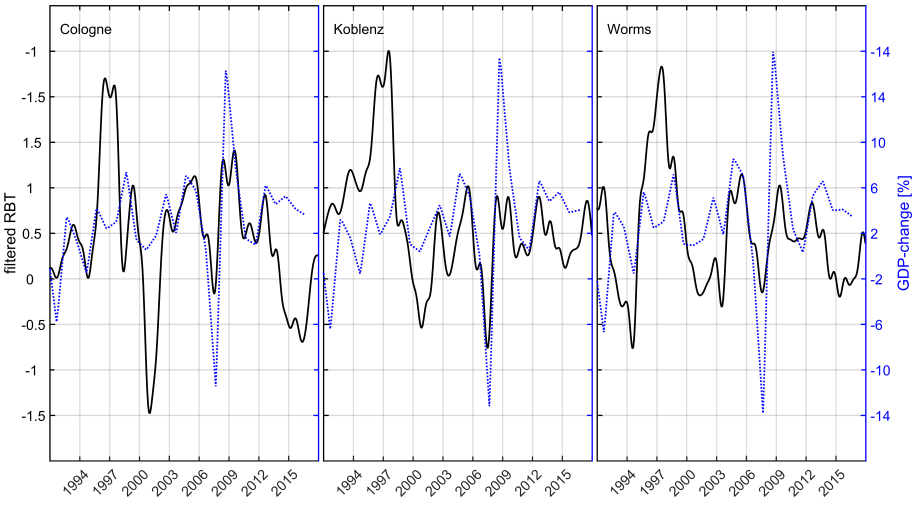

Figure 9. The three panels show the detrended and filtered RBT signal (black solid) and the GDP change (blue dashed) at the Cologne, Koblenz and Worms.

4 Conclusions

We introduce a new catchment-wide air temperature T_c, which decreases the RMSE (Tab. 5) in a $T_c \rightarrow T_w$ regression. T_c is a weighted (ACC*w) average of all T_a across the catchment area including the use of Δt for each grid point according to the hydrological distance and flow speed. This time lag is an indicator when a measured water droplet was at a certain grid cell in the catchment area. As a result, one can get a better estimate which T_a a water droplet experienced on its way to a monitoring station and better linear $T_c \rightarrow T_w$ estimates. This improvement in the $T_c \rightarrow T_w$ relationship supports the analysis, reanalysis and forecast of T_w. Usually T_a data is readily available and can easily be combined with Q data for a multiple linear regression. Still a sufficient long time-series of T_w is required. Nevertheless a linear relationship is simpler than a full physical model which requires all meteorological fluxes as parameters.

This a case study for the Rhine catchment area but the model can be theoretically used in any river system around the globe. Catchment area data and reanalysis T_a data are globally available. Morrill et al. (2005) show a linear $T_a \rightarrow T_w$ relationship for 43 rivers with various catchment areas in the subtropics. This could indicated that this case study of the Rhine can be applied globally. There is a lack of studies on the $T_a \rightarrow T_w$ relationship in the tropics, where precipitation and extreme events, such as monsoon, could complicate this relationship. Future calculations could be coupled with catchment-wide hydrological models to improve the accuracy of the time lag.

Using T_c we regress four T_w time series (Basel, Worms, Koblenz and Cologne) along the Rhine. The offset in the this regression a_1, which we call RBT, and its change over time is an indicator for anthropogenic heat input. The RBT can be correlated with long term economic changes such as the decrease of nuclear power production as well as short term economic events. We show that change in production rates (oil refineries or chemical industry) as well as a change in GDP can influence the RBT

and therefore the Rhine water temperature. Adsitionally, the Spearman's Rank correlation is positive and significant which supports the connection between RBT and GDP. This case study could be on one hand a tool for understanding the long term consequences of industrial water use and on the other hand a verification tool for reported heat input. Germany has a rigorous reporting system on cooling water use. However, other countries could check if industrial heat input is in accordance with legislative guidelines.

Hardenbicker et al. (2016) estimate, using a physical model (QSim), that between the reference period of 1961-1990 and the near future 2021-2050 the mean annual T_w of the Rhine could increase by 0.6 ^{o}C-1.4 ^{o}C. This trend can be supported by our historical data, however they use a constant anthropogenic heat input. Different warming rates along the Rhine could occur by a change in anthropogenic heat input. The difference of the T_w warming rate between Basel and the other monitoring stations in our time-series data can be explained by the change in nuclear power production and the influence of general industrial production. This could mean that with rising T_a and the linear correlation between $T_a \rightarrow T_w$, industrial production and power production have to be more closely connected with river water temperature management. For the Rhine river we find a decreasing, except for Basel, RBT, which indicates a decreasing anthropogenic heat input. However, other river catchment areas with growing energy intensive industries could experience a larger warming rate than it is caused by the general increase of T_a experiencing all consequences for the physical, chemical and biological processes.

References

AG, B.: BASF Geschaeftsbericht, BASF AG Oeffentlichkeitsarbeit und Marktkommunikation 67056 Ludwigshafen Deutschland, 1989.

BAFU: Water temperature and discharge Basel, Bundesamt fuer Umwelt BAFU Abteilung Hydrologie, https://www.bafu.admin.ch, 2019.

Basarin, B., Lukić, T., Pavić, D., and Wilby, R. L.: Trends and multi-annual variability of water temperatures in the river Danube, Serbia, Hydrological Processes, 30, 3315–3329, https://doi.org/10.1002/hyp.10863, 2016.

Benyaha, L., STHilaire, A., Ouarda, T., Bobee, B., and Dumas, J.: Comparison of non-parametric and parametric water temperature models on the Nivelle River France, Hydrological Sciences Journal, 53, 640–655, https://doi.org/10.1623/hysj.53.3.640, 2008.

BfG: Water temperature and discharge Koblenz, Bundesanstalt fuer Gewaesserkunde, Am Mainzer Tor 1, 56068 Koblenz, www.bafg.de, 2019.

Caissie, D.: The thermal regime of rivers: a review, Freshwater Biology, 51, 1389–1406, https://doi.org/10.1111/j.1365-2427.2006.01597.x, 2006.

Delpla, I., Jung, A.-V., Baures, E., Clement, M., and Thomas, O.: Impacts of climate change on surface water quality in relation to drinking water production, Environment International, 35, 1225–1233, http://www.sciencedirect.com/science/article/pii/S0160412009001494, 2009.

Durance, I. and Ormerod, S. J.: Trends in water quality and discharge confound long-term warming effects on river macroinvertebrates, Freshwater Biology, 54, 388–405, https://doi.org/10.1111/j.1365-2427.2008.02112.x, 2009.

Erickson, T. R. and Stefan, H. G.: Linear Air/Water Temperature Correlations for Streams during Open Water Periods, Journal of Hydrologic Engineering, 5, 317–321, https://doi.org/10.1061/(ASCE)1084-0699(2000)5:3(317), https://ascelibrary.org/doi/abs/10.1061/%28ASCE%291084-0699%282000%295%3A3%28317%29, 2000.

Förster, H. and Lilliestam, J.: Modeling thermoelectric power generation in view of climate change, Regional Environmental Change, 10, 327–338, https://doi.org/10.1007/s10113-009-0104-x, 2010.

Garbrecht, J. and Fernandez, G. P.: VISUALIZATION OF TRENDS AND FLUCTUATIONS IN CLIMATIC RECORDS, Journal of the American Water Resources Association, 30, 297–306, https://doi.org/10.1111/j.1752-1688.1994.tb03292.x, 1994.

Haag, I. and Luce, A.: The integrated water balance and water temperature model LARSIM-WT, Hydrological Processes, 22, 1046–1056, https://doi.org/10.1002/hyp.6983, 2008.

Hardenbicker, P., Viergutz, C., Becker, A., Kirchesch, V., Nilson, E., and Fischer, H.: Water temperature increases in the river Rhine in response to climate change, Regional Environmental Change, 17, 299–308, https://doi.org/10.1007/s10113-016-1006-3, 2016.

Hari, R. E., Livingstone, D. M., Siber, R., Burkhardt-Holm, P., and Guettinger, H.: Consequences of climatic change for water temperature and brown trout populations in Alpine rivers and streams, Global Change Biology, 12, 10–26, https://doi.org/10.1111/j.1365-2486.2005.001051.x, 2006.

Hoef, J. M. V. and Peterson, E. E.: A Moving Average Approach for Spatial Statistical Models of Stream Networks, Journal of the American Statistical Association, 105, 6–18, https://doi.org/10.1198/jasa.2009.ap08248, 2010.

Hoef, J. M. V., Peterson, E., and Theobald, D.: Spatial statistical models that use flow and stream distance, Environmental and Ecological Statistics, 13, 449–464, https://doi.org/10.1007/s10651-006-0022-8, 2006.

IAEA: Power Reactor Information System (PRIS), Web, pris.iaea.org/pris/, 2019.

IKSR: Vergleich der Waermeeinleitungen 1989 und 2004 entlang des Rheins, IKSR-Bericht, 2006.

Isaak, D. J., Luce, C. H., Rieman, B. E., Nagel, D. E., Peterson, E. E., Horan, D. L., Parkes, S., and Chandler, G. L.: Effects of climate change and wildfire on stream temperatures and salmonid thermal habitat in a mountain river network, Ecological Applications, 20, 1350–1371, https://doi.org/10.1890/09-0822.1, 2010.

Isaak, D. J., Wollrab, S., Horan, D., and Chandler, G.: Climate change effects on stream and river temperatures across the northwest U.S. from 1980–2009 and implications for salmonid fishes, Climatic Change, 113, 499–524, https://doi.org/10.1007/s10584-011-0326-z, https://doi.org/10.1007/s10584-011-0326-z, 2012.

Isaak, D. J., Peterson, E. E., Hoef, J. M. V., Wenger, S. J., Falke, J. A., Torgersen, C. E., Sowder, C., Steel, E. A., Fortin, M.-J., Jordan, C. E., Ruesch, A. S., Som, N., and Monestiez, P.: Applications of spatial statistical network models to stream data, Wiley Interdisciplinary Reviews: Water, 1, 277–294, https://doi.org/10.1002/wat2.1023, 2014.

Jackson, F., Hannah, D. M., Fryer, R., Millar, C., and Malcolm, I.: Development of spatial regression models for predicting summer river temperatures from landscape characteristics: Implications for land and fisheries management, Hydrological Processes, 31, 1225–1238, https://doi.org/10.1002/hyp.11087, 2017a.

Jackson, F. L., Fryer, R. J., Hannah, D. M., and Malcolm, I. A.: Can spatial statistical river temperature models be transferred between catchments?, Hydrology and Earth System Sciences, 21, 4727–4745, https://doi.org/10.5194/hess-21-4727-2017, 2017b.

Jackson, F. L., Fryer, R. J., Hannah, D. M., Millar, C. P., and Malcolm, I. A.: A spatio-temporal statistical model of maximum daily river temperatures to inform the management of Scotland's Atlantic salmon rivers under climate change, Science of The Total Environment, 612, 1543–1558, https://doi.org/10.1016/j.scitotenv.2017.09.010, 2018.

Koch, H. and Grünewald, U.: Regression models for daily stream temperature simulation: case studies for the river Elbe, Germany, Hydrological Processes, 24, 3826–3836, https://doi.org/https://doi.org/10.1002/hyp.7814, 2010.

Lange, J.: Waermelast Rhein, Bund fuer Umwelt und Naturschutz Deutschland, www.bund-rlp.de/, 2009.

Lehner, B., Verdin, K., and Jarvis, A.: New Global Hydrography Derived From Spaceborne Elevation Data, Eos, Transactions American Geophysical Union, 89, 93, https://doi.org/10.1029/2008eo100001, https://doi.org/10.1029/2008EO100001, 2008.

LfU: Water temperature and discharge Worms, Landesamt fuer Umwelt Rheinland-Pfalz, https://lfu.rlp.de/, 2019.

Markovic, D., Scharfenberger, U., Schmutz, S., Pletterbauer, F., and Wolter, C.: Variability and alterations of water temperatures across the Elbe and Danube River Basins, Climatic Change, 119, 375–389, https://doi.org/10.1007/s10584-013-0725-4, 2013.

Mohseni, O., Stefan, H. G., and Erickson, T. R.: A nonlinear regression model for weekly stream temperatures, Water Resources Research, 34, 2685–2692, https://doi.org/10.1029/98WR01877, 1998.

Morrill, J. C., Bales, R. C., and Conklin, M. H.: Estimating Stream Temperature from Air Temperature: Implications for Future Water Quality, Journal of Environmental Engineering, 131, 139–146, https://doi.org/10.1061/(asce)0733-9372(2005)131:1(139), https://doi.org/10.1061/(ASCE)0733-9372(2005)131:1(139), 2005.

MWV: Mineraloel und Raffinerien, Mineraloelwirtschaftsverband e.V., 2003.

Peterson, E. E. and Hoef, J. M. V.: A mixed-model moving-average approach to geostatistical modeling in stream networks, Ecology, 91, 644–651, https://doi.org/10.1890/08-1668.1, 2010.

Piccolroaz, S., Calamita, E., Majone, B., Gallice, A., Siviglia, A., and Toffolon, M.: Prediction of river water temperature: a comparison between a new family of hybrid models and statistical approaches, Hydrological Processes, 30, 3901–3917, https://doi.org/10.1002/hyp.10913, 2016.

Pohle, I., Helliwell, R., Aube, C., Gibbs, S., Spencer, M., and Spezia, L.: Citizen science evidence from the past century shows that Scottish rivers are warming, Science of The Total Environment, 659, 53–65, https://doi.org/10.1016/j.scitotenv.2018.12.325, 2019.

Sinokrot, B. A. and Stefan, H. G.: Stream temperature dynamics: Measurements and modeling, Water Resources Research, 29, 2299–2312, https://doi.org/10.1029/93WR00540, 1993.

Stefan, H. G. and Preud'homme, E. B.: STREAM TEMPERATURE ESTIMATION FROM AIR TEMPERATURE, Journal of the American Water Resources Association, 29, 27–45, https://doi.org/10.1111/j.1752-1688.1993.tb01502.x, 1993.

Tobler, W. R.: A Computer Movie Simulating Urban Growth in the Detroit Region, Economic Geography, 46, 234, https://doi.org/10.2307/143141, 1970.

Toffolon, M. and Piccolroaz, S.: A hybrid model for river water temperature as a function of air temperature and discharge, Environmental Research Letters, 10, 114 011, https://doi.org/10.1088/1748-9326/10/11/114011, 2015.

VGdL, A.: Bruttoinlandsprodukt, Bruttowertschoepfung in den Laendern der Bundesrepublik Deutschland, Revision 2014, www.statistik-bw.de/VGRdL, 2019a.

VGdL, A.: Rueckrechnungsergebnisse fuer das frueherer Bundesgebiet, Revision 2005, www.statistik-bw.de/VGRdL, 2019b.

Webb, B. W. and Nobilis, F.: Long term water temperature trends in Austrian rivers, Hydrological Sciences Journal, 40, 83–96, https://doi.org/10.1080/02626669509491392, https://doi.org/10.1080/02626669509491392, 1995.

Webb, B. W. and Nobilis, F.: LONG-TERM PERSPECTIVE ON THE NATURE OF THE AIR–WATER TEMPERATURE RELATIONSHIP: A CASE STUDY, Hydrological Processes, 11, 137–147, https://doi.org/10.1002/(SICI)1099-1085(199702)11:2<137::AID-HYP405>3.0.CO;2-2, 1997.

Webb, B. W., Clack, P. D., and Walling, D. E.: Water-air temperature relationships in a Devon river system and the role of flow, Hydrological Processes, 17, 3069–3084, https://doi.org/10.1002/hyp.1280, 2003.

Wenger, S. J., Isaak, D. J., Dunham, J. B., Fausch, K. D., Luce, C. H., Neville, H. M., Rieman, B. E., Young, M. K., Nagel, D. E., Horan, D. L., and Chandler, G. L.: Role of climate and invasive species in structuring trout distributions in the interior Columbia River Basin, USA, Canadian Journal of Fisheries and Aquatic Sciences, 68, 988–1008, https://doi.org/10.1139/f2011-034, 2011.

WSA: Water temperature and discharge Cologne, Wasserstraßen- und Schifffahrtsamt Duisburg-Rhein, http://www.wsa-duisburg-rhein.wsv.de, 2019.

Yamarone, R.: Indexes of Leading, Lagging, and Coincident Indicators, John Wiley and Sons, Inc., https://doi.org/10.1002/9781118532461.ch2, 2012.

Zhu, S., Heddam, S., Nyarko, E. K., Hadzima-Nyarko, M., Piccolroaz, S., and Wu, S.: Modeling daily water temperature for rivers: comparison between adaptive neuro-fuzzy inference systems and artificial neural networks models, Environmental Science and Pollution Research, 26, 402–420, https://doi.org/10.1007/s11356-018-3650-2, 2018.